Exp Fluids (2009) 46:725–736
DOI 10.1007/s00348-008-0604-3

RESEARCH ARTICLE

Non-invasive measurement of void fraction and liquid temperature in microchannel flow boiling

David Fogg · Milnes David · Kenneth Goodson

Received: 30 January 2008 / Revised: 12 November 2008 / Accepted: 21 November 2008 / Published online: 27 December 2008

Abstract Past thermometry research for two-phase microfluidic systems made much progress regarding wall temperature distributions, yet the direct measurement of fluid temperature has received little attention. This paper uses a non-invasive two-dye/two-color fluorescent technique to capture fluid temperature along with local liquid fraction in a two-phase microflow generated by injecting air into a heated microchannel. The fluorescent emission of Rhodamine 110 and Rhodamine B, measured with photodiodes, is used to obtain local liquid temperature (±3°C) and void fraction (±2% full-scale) over a temperature range from 45 to 100°C. Arrays of these sensors can significantly expand the set of measurable flow parameters to include bubble/slug frequency, size, velocity, and growth rates in addition to mapping the local liquid temperature and void fraction.

List of symbols

α	void fraction
β	liquid fraction
ε	perturbation in signal
κ	extinction coefficient of H_2O (m^{-1})
ξ	intensity constant group (W m)
σ	surface tension (N m^{-1})
ϕ	quantum efficiency
Φ	quantum efficiency constant group (m^{-1})
a	molar extinction coefficient (L mol^{-1} m^{-1})
A	area (m^2)
c	concentration (mol L^{-1})
d	diameter (m)
H	channel depth (m)
E	error
I	incident intensity (W m^{-2})
p	pressure (N m^{-2})
P	power (W)
$\hat{P}$	normalized Power
T	temperature (°C)
T	transmittance
t	time (s)
V	voltage (V)

Subscripts

λ,inc	incident wavelength
a	absorbed
d	detected
dye	property of a dye
e	emitted
fo	all liquid
g	glass
go	all vapor
m	measurement
ref	reference value
PD	photodiode
PRED	predicted
TC	thermocouple

D. Fogg (✉)
Creare Inc.,16 Great Hollow Rd, Hanover, NH 03755, USA
e-mail: dwf@creare.com

M. David · K. Goodson
Department of Mechanical Engineering, Stanford University, Building 530, Room 224, Stanford, CA 94305-3030, USA

1 Introduction

The study of two-phase microfluidics has received significant attention over the past two decades. Micro-sized heat

pipes (Mallik et al. 1992), jets (Wang et al. 2002; Brunschwiler et al. 2006), and heat exchangers (Zhang et al. 2002) are being studied widely as cooling solutions for a variety of electronic devices including integrated circuits and radiation sources. Due to the size of the microchannels, metrology in past experimental work has been restricted to wall temperatures, inlet and exit pressures, and digital imaging. To support the development of analytical models, measurement techniques for local void fraction, pressure, and liquid temperature need to be developed.

Analytical and numerical models for microscale two-phase flows have begun to appear. Jacobi and Thome (2002) modeled the heat transfer from elongated bubbles in microchannel flows, Qu and Mudawar (2003) analyzed the heat transfer in annular two-phase microchannel flows, and Yarin et al. (2002) studied two-phase capillary flow with phase change at the meniscus. Koo et al. (2001) developed a one-dimensional steady-state numerical model for boiling microchannel flows. Unfortunately, due to the lack of data and metrology methods, numerical and analytical models are difficult to verify. To construct accurate models of microchannel flows, the metrology needs to be developed for local parameters such as void fraction, pressure, and liquid temperature. Voids are particularly important as they are indicative of the flow regimes and heat and mass transfer.

Traditional void fraction measurement techniques are difficult to implement in microchannels. Due to the small dimensions of the microchannels, invasive techniques such as hot wire anemometry are not applicable because the probes influence the flow distributions. Non-invasive techniques like gamma densitometry or X-ray tomography are impractical due to cost, space, and/or lab safety constraints. Capacitive sensors, which take advantage of the significant differences between the dielectric constants of the two phases, are promising but difficult to calibrate due to the signal dependence on both overall void fraction and flow regime (Chaouki et al. 1997). Keska (2005) compared the simultaneous void measurements for capacitive and conductive sensors in microchannels and found that more than 50% of the points were not in agreement to within ±15% of each other. Void fractions have been reported in triangular micro heat pipes using capacitive sensors (Lee et al. 2003), but the behavior of capacitive sensors for highly transient flow has yet to be well characterized. Ide et al. (Ide 2006) developed an optical system to measure void fraction using the transmission of infrared light across the channel and observed reasonable success for isothermal air–water systems. Cross-correlation between neighboring probes yielded slug length and velocity.

To date, temperature measurements for two-phase microflows have been limited to wall temperatures. Researchers have utilized a number of techniques to measure wall temperatures. Embedded thermocouples (Qu and Mudawar 2003; Wu and Cheng 2004, Xu et al. 2004) or micromachined thermistors (Zhang et al. 2002, Lee et al. 2003) are the most common approaches for microchannel flow boiling temperature measurements. Arrays of these sensors provide axial wall temperature distributions. Hollingsworth (2004) imaged the two-dimensional temperature field on the backside of a microchannel array using thermochromic liquid crystals. The liquid crystals display a range of colors depending on the temperature, where red is at the lower end of the temperature range and blue is at the high end. Other researchers, such as Narayanan (2003), used IR thermography to measure microchannel wall temperatures.

Fluorescence has been used for optical measurements of temperature in micro-geometries (Barton and Tangyunyong 1996; Ross et al. 2001; Kim et al. 2003). The intensity of the emitted light depends on the temperature of the fluorescent dye allowing measurements accurate to within 1°C. Fluorescence has also been used to measure void fraction. Angelini et al. (1992) used such a technique for macroscale dispersed droplet flows. This technique has also been used in fuel vaporization studies (Bazile and Stepowski 1994). Fogg et al. (2004) demonstrated void fraction in isothermal microflows can be measured using single dye fluorescence.

The present work develops a two-dye/two-color fluorescent technique to measure void fraction and liquid temperature in confined flow boiling. The theory indicating the fluorescent emission depends on both temperature and void fraction is presented. The temperature dependent emission for each dye is calibrated for single phase flow, while the ability to measure void fraction is characterized for a room temperature air–water flow. The technique is then applied to flows with varying temperature and void fraction to evaluate the ability to simultaneously measure the two parameters. Two-dye/two-color fluorescence provides a unique opportunity to measure liquid temperature and void fraction in microchannels and arrays of sensors are expected to yield additional information such as bubble and slug length, frequency, velocity, and perhaps growth rates.

2 Measurement principle

Fluorescence is a luminescence phenomenon in which a molecule becomes energized by absorbing a photon and subsequently emits another photon, generally of different wavelength. Since some of the absorbed energy is lost to collisions with neighboring molecules, the emitted radiation experiences a Stokes shift to a longer wavelength than the excitation radiation (Guilbault 1990). Not all absorbed

radiation results in an emitted photon at the fluorescent wavelength. The ratio of emission to absorption, known as the quantum efficiency, ϕ, is generally a function of temperature. Given that the time the molecule stays in the excited state is typically short ($\sim 10^{-9}$ s) high speed measurements of transient phenomena are possible.

Fluorescent techniques can capture rapid changes in the local void fraction and significantly improve the characterization of flow regimes in microchannels. High-speed digital imaging is effective but is also expensive and cumbersome considering data storage and retrieval. At sampling rates sufficient to avoid aliasing, sampling duration is often limited to only a few seconds and key flow regime transitions may remain unobserved if long transients exist (Wu and Cheng 2003, 2004; Xu et al. 2004). Processing images is extremely time consuming, thereby limiting the use of digital imaging as a quantitative tool. One major downside to digital imaging is the inability to present full transient data sets in archival publications. Researchers use only a few images to support their observations. For any highly transient complex flow the limited sequences will under sample the phenomenon for the readers preventing them from drawing their own conclusions based on the actual data.

Fluorescence has been used to separately measure both temperature and void fraction (Angelini et al. 1992; Bazile and Stepowski 1994; Barton and Tangyunyong 1996; Ross et al. 2001). Using two dyes that emit at different wavelengths that can be measured with two separate optical detectors, such as photodiodes or CCD arrays, both the temperature and liquid fraction of the measurement volume can be calculated. In this study, Rhodamine B and Rhodamine 110 serve as an appropriate dye pair. The absorption and emission spectra for these dyes are shown in Fig. 1.

A one-dimensional analysis for a single dye reveals the dependence of the detected intensity of the emitted wavelength on the temperature and liquid fraction of the measurement volume. Assuming scattering, reflection, and refraction can be neglected, the power absorbed is

$$P_a = \mathrm{IAT}_g(1 - \exp(\bar{a}_{\lambda,\mathrm{inc}} H\beta)) \tag{1}$$

$$\bar{a}_{\lambda,\mathrm{inc}} = \kappa_{\lambda,\mathrm{inc}} + c a_{\lambda,\mathrm{inc,dye}} \tag{2}$$

where P_a is the power absorbed by the dye solution, I is the intensity of the excitation light on the microchannel, T_g is the transmittance of the glass cover, A is the area of the channel illuminated, κ is the extinction coefficient of water, a is the molar extinction coefficient of the dye, H is the depth of the channel, β is the volume averaged liquid fraction, and c is the molar concentration of the dye. If $\bar{a}_{\lambda,\mathrm{inc}} H\beta \ll 1$, the optically thin assumption is valid such that $\exp(-\bar{a}_{\lambda,\mathrm{inc}} H\beta) \approx 1 - \bar{a}_{\lambda,\mathrm{inc}} H\beta$, which allows the absorbed power in the dye to be expressed as

$$P_{a,\mathrm{dye}} \approx \mathrm{IAT}_g c_{\mathrm{dye}} a_{\lambda,\mathrm{inc,dye}} H\beta \tag{3}$$

Given the quantum efficiency of the dye, the fluorescent power emitted is

$$P_e = \mathrm{IAT}_g c_{\mathrm{dye}} a_{\lambda,\mathrm{inc,dye}} H\beta\phi_{\mathrm{dye}} \tag{4}$$

Assuming the fluid is also optically thin for the emitted fluorescence, the power absorbed by the detector after transmission back through the two-phase mixture and the glass is

$$P_d \approx \mathrm{IAT}_g^2 c_{\mathrm{dye}} a_{\lambda,\mathrm{inc}} H\beta\phi_{\mathrm{dye}} = \xi\Phi\beta \tag{5}$$

where $\xi = \mathrm{IAT}_g^2 c_{\mathrm{dye}} H$ can be treated as a constant with respect to temperature, while $\Phi = a_{\lambda,\mathrm{inc,dye}}\phi_{\mathrm{dye}}$ is a function of temperature.

It is helpful to remove the dependence on the incident intensity and dye concentration from the measurement. This can be achieved by normalizing the data for a given run by measurements at a known temperature, $\mathrm{T}_{\mathrm{ref}}$, and liquid fraction, $\beta = 1$.

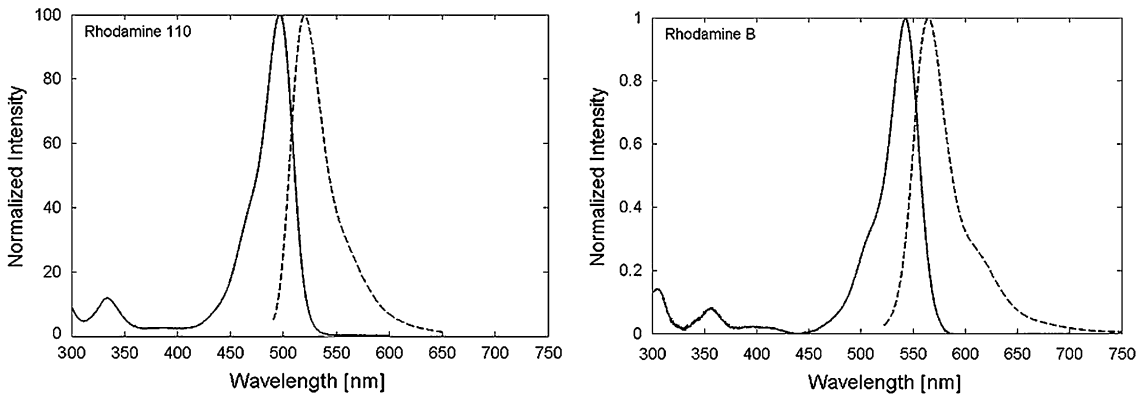

Fig. 1 Absorption and emission spectra for Rhodamine 110 and Rhodamine B (OmegaFilters, 2007)

$$\hat{P} = \frac{P_d(\mathsf{T}, \beta)}{P_d(\mathsf{T}_{\text{ref}}, 1)} = \frac{\Phi(\mathsf{T})\beta}{\Phi(\mathsf{T}_{\text{ref}})} \tag{6}$$

Equation 6 assumes that the light source is spatially uniform and temporally stable and the dye concentration is uniform throughout the run. Reflection and refraction from the curved bubble surfaces are also neglected. For isothermal flows, only a single dye is required. The temperature dependence drops out and the normalized power is the liquid fraction, $\hat{P} = \beta$. For heated flows, two dyes are required. Solving Eq. 6 for liquid fraction for each dye obtains

$$\beta = \hat{P}_1 \frac{\Phi_1(\mathsf{T}_{\text{ref}})}{\Phi_1(\mathsf{T})} = \hat{P}_2 \frac{\Phi_2(\mathsf{T}_{\text{ref}})}{\Phi_2(\mathsf{T})} \tag{7}$$

which can be rearranged as

$$\frac{\Phi_1(\mathsf{T})}{\Phi_2(\mathsf{T})} = \frac{\hat{P}_1}{\hat{P}_2} \frac{\Phi_1(\mathsf{T}_{\text{ref}})}{\Phi_2(\mathsf{T}_{\text{ref}})} \tag{8}$$

In Eq. 8, the normalized powers are experimental values, while $\Phi_1(\mathsf{T}_{\text{ref}})$ and $\Phi_2(\mathsf{T}_{\text{ref}})$ are obtained from the calibration curves of dye 1 and dye 2 respectively. This provides a value for $\Phi_1(\mathsf{T})/\Phi_2(\mathsf{T})$ which allows the temperature of the liquid in the measurement volume to be determined from the ratio of the calibration curves for the two dyes. An example of these calibration curves is provided in Fig. 5. Once the temperature has been determined, Eq. 7 can be used to calculate the liquid fraction.

The one-dimensional analysis neglects several potential sources of error. If the light source is not spatially uniform as is assumed, the location of the void within the measurement volume will affect the result. Local variations in the concentration of the dye are another source of uncertainty, particularly for rapidly boiling flows. If the dye does not vaporize with the liquid higher concentrations could develop in the vicinity of the interface. The intensity of the incident light may also affect the accuracy of the measurement. Under high-intensity illumination, a permanent destruction of fluorophores, known as photobleaching, may occur reducing the emitted radiation.

The reflection and refraction of light due to the curved liquid-vapor interface poses yet another source of error. The reduction in the excitation intensity on liquid beneath these interfaces will be negligible particularly for bubbles contained completely within the measurement volume. For small bubbles, the reflected and refracted light from adjacent regions of the measurement volume will compensate for any line-of-sight losses. In annular flows, the curvature only exists in the transverse direction. For this case, light will be redirected across the channel minimizing losses in the streamwise direction. Large slugs with only the front or back interface in the measurement volume provide the largest source of error due to reflections and refractions. The streamwise curvature leads to losses down the length of the channel.

Similar results are expected for the reflections and refractions of the emitted light. The reflected light often creates bright rings around bubbles. The ring results from light emitted from neighboring regions which are reflected and refracted towards the detector. This local increase poses problems primarily for point measurements with a CCD array in the vicinity of the interface. At the cost of spatial resolution, volume-averaged measurements will be more accurate as the light collected is emitted from within the measurement volume. In volume-averaged measurements, the error is minimized for smaller bubbles because the solid angle which the detector occupies is large and most of the light is collected. As the bubble gets larger, the solid angle decreases, thereby increasing the losses.

3 Dye selection

Selection of a compatible pair of dyes is crucial to the technique. The absorption and emission spectra need to be distinct with minimal crosstalk and the temperature dependent emission ratio must be monotonic. Ideally one dye would have no temperature dependence and the other would vary significantly. The dye with no temperature dependence could be used solely for the void fraction measurement while the other would be used for the local liquid temperature.

Two-dye/two-color fluorescence has been used to improve the resolution of liquid temperature measurements. Sakakibara and Adrian (1999) used Rhodamine B and Rhodamine 110 to resolve whole field temperatures in water to within 1.4 K. They refined the technique further by taking into consideration blurring between image pairs to improve the accuracy to 0.17 K (Sakakibara and Adrian 2004). This study utilizes Rhodamine B and Rhodamine 110.

Alternatives to this dye pair, including single dye/two-color emission, exist in the literature. Researchers such as Bruchhausen (Bruchhausen et al. 2005) and Lavieille et al. (2001) used two spectral bands in the emission of Rhodamine B to measure liquid temperature in an approach similar to the two dye technique. Adding a third spectral band (Lavieille et al. 2004) to the Rhodamine B measurement allows the functional dependence of parameters such as probe volume size, dye concentration, and Beer's absorption to be eliminated. The three band technique has been used to measure the temperature of acetone-ethanol binary droplets in which the droplet composition varies with time (Maqua et al. 2006).

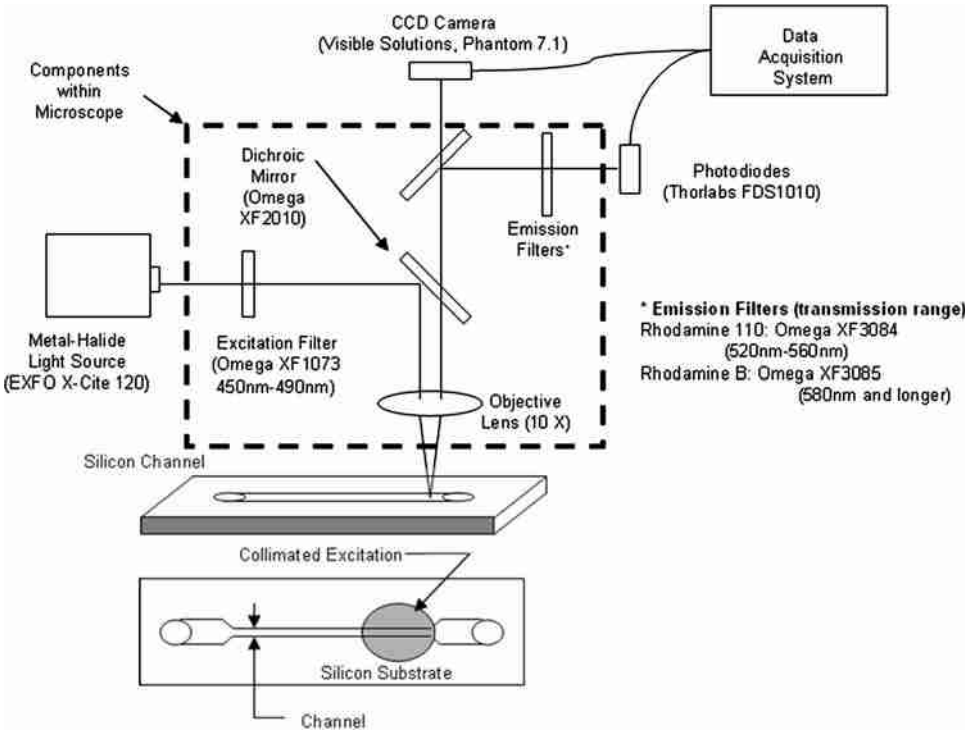

Fig. 2 Schematic of the optical setup

4 Experimental apparatus

4.1 Optical setup

Figure 2 shows a schematic of the optical equipment used to simultaneously measure void fraction and liquid temperature. In this setup, the emission from a metal-halide lamp (EXFO: X-Cite 120) travels through an excitation filter (Omega: XF1073) and reflects off a dichroic mirror (Omega: XF2010) to allow only light from 450–490 nm into the measurement volume. The microchannel is magnified using a Nikon Plan Fluor 10X objective with a numerical aperture of 0.30 and a working distance of 16 mm. The optical interrogation window measures 1.3 mm long by 0.5 mm wide. The emitted light passes back through the dichroic mirror. The optics in the microscope split the emitted beam to the two eyepieces. Attached to each eyepiece is an emission filter for one of the dyes and a large area photodiode (Thorlabs: FDS1010). For Rhodamine 110, the emission filter (Omega: XF 3084) allows light from 520–560 nm to reach the photodetector, while for Rhodamine B, the filter (Omega: XF3085) transmits light with wavelengths longer than 580 nm. The microscope can also be configured to image the flow using a CCD camera (Visible Solutions: Phantom 7.1). The images are used to visually characterize the flow regimes and bubble frequencies recorded by the photodiodes. The CCD camera is not used for the fluorescent measurements.

4.2 Fluidic and heating configurations

A schematic of the fluidic path and the heating components is shown in Fig. 3. The two dye solution of 50 μM Rhodamine B and 50 μM Rhodamine 110 is driven by a syringe pump (Harvard Apparatus: PHD2000). The resulting liquid flow rate and pressure drop are monitored by a liquid flow sensor (Omega: FLR-1602A) and pressure transducer, (Omega: PX01C1-015G5T), respectively. The inlet and outlet fluid temperatures to the microchannel are measured using K-type thermocouples (Omega: 5TC-TT-K-36), accurate to within 1.1 K, inserted into the flow exiting the channel manifolds. The fluorescent measurement is made within 1 mm of the exit thermocouple. In the

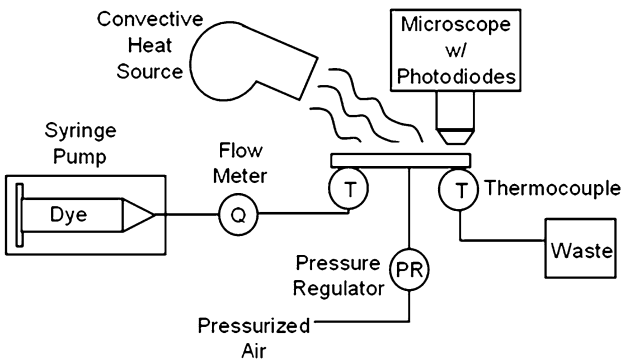

Fig. 3 Schematic of the fluidic and heating components in the experimental verification

single channel device, bubbles are generated by supplying air at a known pressure through an orifice similar in size to the cavities being fabricated as nucleation sites in some microchannel experiments (Kosar et al. 2005; Kandlikar et al. 2006a, b). The air pressure is set with the pressure regulator. The pressure needs to be large enough to overcome the surface tension force at the air–liquid interface as given by the Young–LaPlace equation.

$$p_b \geq p_f + \frac{4\sigma}{d} \tag{9}$$

Once air begins to flow, bubbles and slugs are generated from the small air orifice. The two-phase mixture exits the device and goes to a waste container which has the option of being pressurized or remaining at atmospheric pressures. The high speed camera, records the flow at rates of 5,000 frames per second. A variable power convection source is used to heat the microdevice to a set of steady state temperatures. A range of temperatures can be achieved as the device cools by natural convection. As indicated by a low Biot number ($Bi \approx 4 \times 10^{-5}$), the chip is uniform in temperature as it cools. The cooling process typically takes about 10 min to go from 100 to 35°C.

4.3 Device fabrication

The process flow for the fabrication of the microchannel is shown in Fig. 4. (a) It starts with a 350 μm thick double-side polished n-type <100> silicon wafer. A 7 μm thick photoresist (SPR 220-7) is spun on the wafer to pattern the microchannel etch. (b) A deep reactive ion etch (STS multiplex ICP) is performed to etch microchannels 100 μm deep. (c) The wafer is flipped to pattern the water inlet/outlet with 10 μm photoresist on the wafer backside to create access to the microchannels. The through etch is achieved using deep reactive ion etching. The air inlet for bubble generation is etched in the same step. (d) Because the opening for water inlet/outlet (1 mm) is much larger than the opening for air inlet (~15 μm), the etch rate of water inlet/outlet is also much larger than that of the air inlet. Teflon tape is applied to cover the water inlet/outlet once they punch through to continue etching the air inlet till it goes through. (e) After the etch is complete, the wafer is cleaned with a mixture of piranha and oxygen plasma prior in preparation for anodic bonding. (f) The finished silicon wafer is anodically bonded with an ultrasonically cleaned 500 μm thick Pyrex 7740 glass wafer. The bonded stack is diced with a wafer saw to separate the individual channel structures. The devices are ready for packaging with inlet/outlet ports for connection with 250 μm inner diameter tubing. The channel used in this experiment measures 500 μm wide, 100 μm deep, and 2.5 cm long. The overall dimension of the silicon device is 3.5 cm long by 9.5 mm wide.

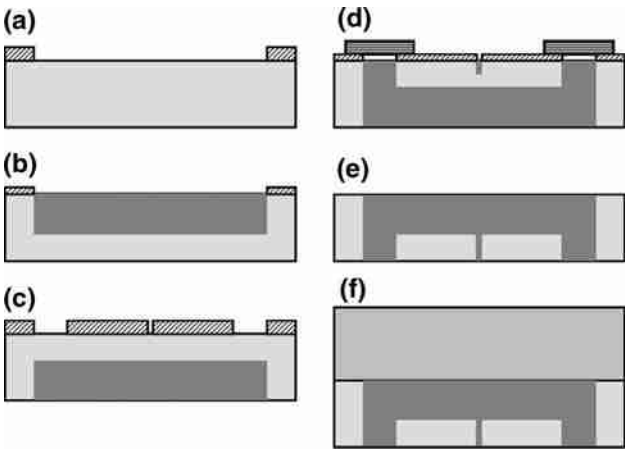

Fig. 4 Device fabrication process: (**a**) deposit and pattern 7 μm photoresist. (**b**) Deep reactive ion etch (DRIE) channels 25-μm deep. (**c**) Flip wafer and pattern the inlet/outlet ports with 10 μm photoresist. (**d**) Etch (DRIE) ports through to channel. The etch rate of water inlet/outlet is larger than that of air inlet. A Teflon tape covers the water inlet/outlet once they etch through. (**e**) Continue etch until air inlet punches through, followed by wafer clean step. (**f**) Anodic bond Pyrex 7740 glass wafer

5 Results and discussion

5.1 Liquid temperature calibration

The temperature calibration is performed using the experimental setup depicted in Figs. 2 and 3. The silicon device is heated by the convective heat source to a constant temperature determined by the heater power and losses to the environment. The heater is turned off and the device is allowed to cool by natural convection.

The small Biot number for the silicon channel indicates the silicon substrate is isothermal. The heat transfer from the constant temperature wall to the fluid raises the temperature of the incoming liquid to the wall temperature within the first 1 mm of the silicon channel. Since the optical probe is located just upstream of the exit manifold where the liquid temperature is measured by the outlet thermocouple inside the tip of the outlet tube, the temperature associated with the two dye fluorescent emission can be calibrated with the exit temperature as the device cools.

The temperature sensitivities for Rhodamine B and Rhodamine 110 are shown in Fig. 5. Rhodamine 110 is fairly temperature independent over a range of 40–100°C with the signal intensity decreasing by only 10%. The emission of Rhodamine B, on the other hand, varies significantly with temperature. The fluorescent emission decreases almost 45% over the same temperature range.

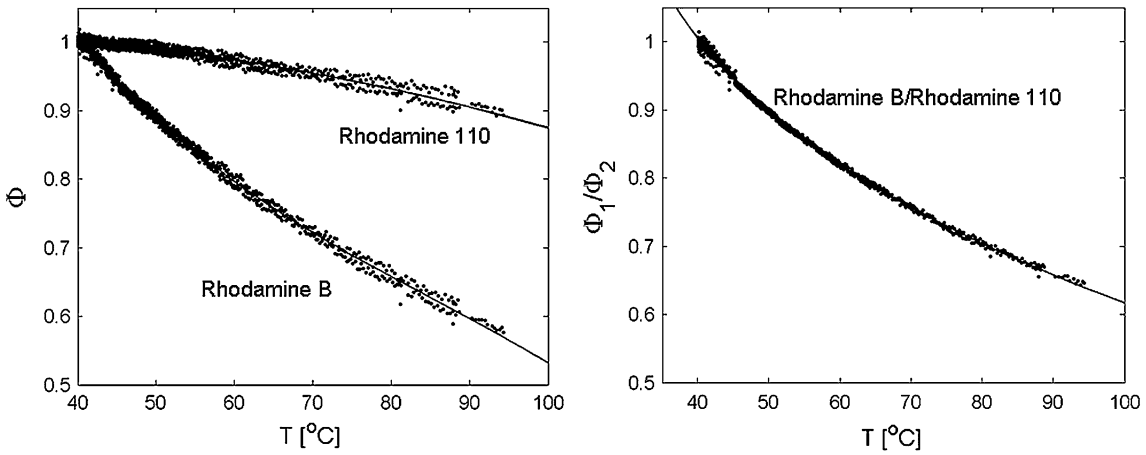

Fig. 5 Temperature calibration for Rhodamine B, Rhodamine 110, and the ratio of the two curves

The normalized temperature dependence for each of these dyes has been fit to a third-order polynomial with Rhodamine B given by

$$\Phi_1(T) = -1.1398E-6T^3 + 2.9255E-4T^2 - 0.0310T + 1.8459 \quad (10)$$

and Rhodamine 110 as

$$\Phi_2(T) = -2.8337E-8T^3 - 1.2367E-5T^2 + 2.2326E-5T + 1.0208 \quad (11)$$

The ratio of these two curves monotonically decreases with an average slope of 0.65% per Kelvin. The decreasing slope as temperature increases yields lower accuracy at higher temperatures. The temperature in °C corresponding to the ratio of the normalized powers is given by

$$T = -143.0208\left(\frac{\Phi_1}{\Phi_2}\right)^3 + 583.0679\left(\frac{\Phi_1}{\Phi_2}\right)^2 - 812.7896\left(\frac{\Phi_1}{\Phi_2}\right) + 413.1936 \quad (12)$$

Correlation coefficients of 0.992, 0.987, and 0.999 for Eqs. 10, 11, and 12 respectively indicate the fits represent the physical dependence over the calibrated temperature range well.

5.2 Isothermal void fraction measurements

The ability to resolve void fraction is evaluated for a homogeneous flow in a 1/8 in ID circular tube. A syringe pump is used to continuously deliver known ratios of air and liquid through a clear plastic tube as depicted in Fig. 6. A T-junction is used to create alternating slugs of liquid and vapor. To ensure that the delivery of air is approximately constant, a pressure sensor on the air line is monitored to determine when the air pressure has stabilized to within 0.1 psi. The flow rates are selected to guarantee

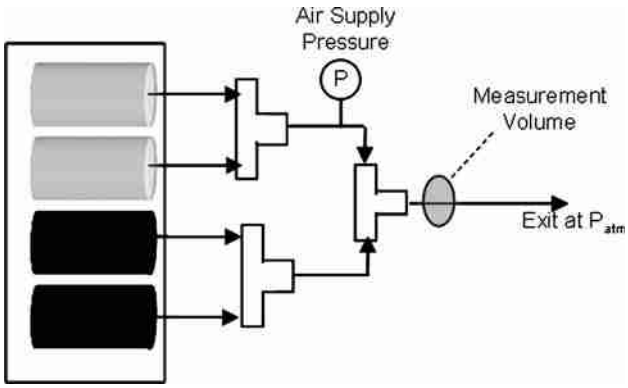

Fig. 6 Schematic of the fluidic system for the isothermal transient void measurements

the supply air pressure is no more than 1.0 psi above atmospheric to minimize expansion of the vapor within the measurement tube. The pump is capable of carrying four syringes at once.

For this void fraction calibration, the vapor bubbles span the full width of the cross section, with the exception of a very, very thin liquid film at the walls. The superficial mixture velocity of 0.02 m/s corresponds to a Reynolds number of 64 and a Weber number of 0.02. According to Tong (1995), there are three effects that cause the vapor flow to slip relative to the liquid: bouyancy, non-uniform void distribution across the channel cross section, and the Bernoulli effect where rapidly expanding flow causes the two phases to accelerate differently. The low Weber number indicates surface tension dominates over the liquid interia and the shape of the liquid vapor interface should not change significantly due to the flow. The overwhelming strength of surface tension prevents the liquid film from thickening as the mixture passes through the tube and past the sensor. Consequently, the void spans the entire width of

the channel negating slip due to non-uniform void distribution. The horizontal orientation eliminates bouyancy effects and there are no expansion or contractions near the measurement volume. The lack of all three effects known to cause void to slip ensures the vapor and liquid move at the same velocity and behaves as a homogeneous flow. The low flow velocity is nearly analogous to a stationary liquid vapor mixture over which the sensor traverses. By using different numbers of syringes to deliver liquid and air, void fractions of 0, 1/4, 1/3, 1/2, 2/3, 3/4, and 1 are possible.

The time-averaged liquid fraction is determined from the ratio of identical syringes dedicated to air and liquid for each run. Assuming the liquid-vapor mixture within the measurement tube moves at a constant velocity, the integration of the signal is used to calculate the time-averaged liquid fraction using Eq. 13

$$\beta = \frac{\bar{V}_m - V_{go}}{V_{fo} - V_{go}} \tag{13}$$

where $\bar{V}_m$ is the time average of the signal from the photodiode, while V_{go} and V_{fo} are the photodiode voltages when the channel is completely filled with gas or liquid respectively.

Figure 7 displays a transient signal from the photodiode for a predicted liquid fraction of $\beta = 0.5$. The flat peaks are liquid slugs which are completely within the measurement volume. The linear increases and decreases between the local minima and maxima are the result of the slugs moving at a constant velocity into and out of the measurement volume.

For the measurements, the supply air pressure was limited to 1.0 psi above atmospheric which restricts the expansion of the vapor within the exit tube to less than 6.8%. For the worst case of $\beta = 0.25$, this translates to a maximum error for the time-averaged liquid fraction of 1.2% due to expansion if the measurement is taken just prior to the tube exit. The measurements are always taken within the first third of the tube to minimize this error.

As shown in Fig. 8, the time-averaged photodiode signal is in good agreement with the predicted liquid fraction

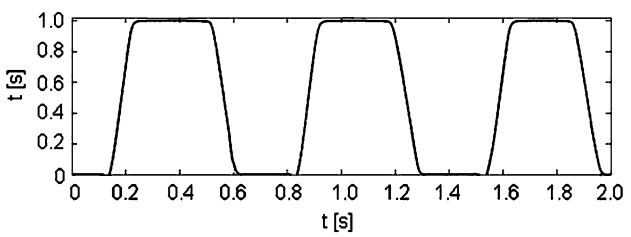

Fig. 7 A sample of the transient photodiode signal for a run in which the predicted liquid fraction is 0.5

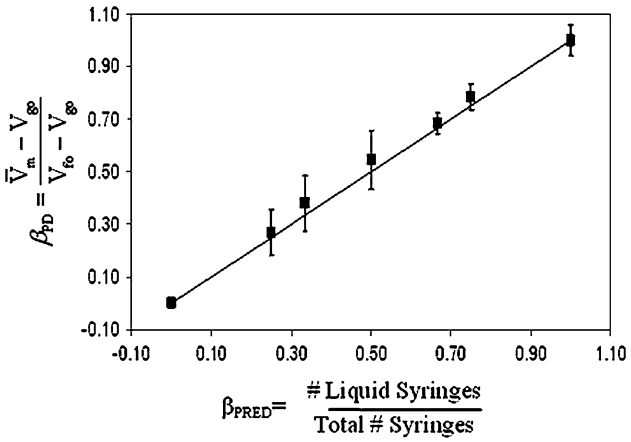

Fig. 8 Comparison of the time-averaged liquid fraction measured by the photodiode to the predicted delivered void fraction

given the ratio of tubes dedicated to liquid and vapor delivery. The two-sigma error bars represent the repeatability of the measurements after breaking down and reassembling the pump setup in Fig. 6. Each data point represents the mean of ten independent experimental observations, where each observation is the time average over 300 s. The mean measurements for each dye agree with each other to within 2% of the full scale.

The supply air pressure is also monitored to ensure that a steady state value is achieved to within 0.1 psi. However, a true steady state is not always achieved. A pressure instability is observed in some measurements in which the size of the vapor slugs would grow larger and the velocity of the mixture in the tube would visibly increase as the air supply pressure increased. At some point, the velocity of the liquid–vapor mixture has increased enough such that air supply pressure decreases and the cycle repeats. This introduces additional error in the measurement as the measured void assumes the liquid and vapor spends equal time in the measurement volume. The magnitude of the pressure instability increases with an increase in the volume of the air supply as is evident by the decline in the repeatability of the measurements at the lower liquid fractions.

Obtaining void fraction from fluorescence has a number of advantages over digital imaging. As seen in Fig. 9, fluorescence allows fluctuations in void to be captured over long periods of time. Both qualitative and quantitative information is readily extracted from the signal. High sampling rates minimize the potential for signal aliasing. Memory requirements are minimal compared to image storage as is the time required to compute the void fraction. The point signal can be plotted in a single plot allowing the data to be easily disseminated in archival publications. The disadvantage of the fluorescent signal is that fluctuations in the signal can be misinterpreted. For example, closely

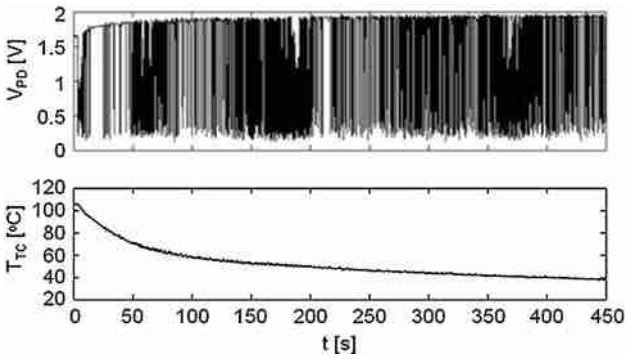

Fig. 9 Time traces of the Rhodamine 110 photodiode voltage and the thermocouple temperature during a calibration cycle with air injection

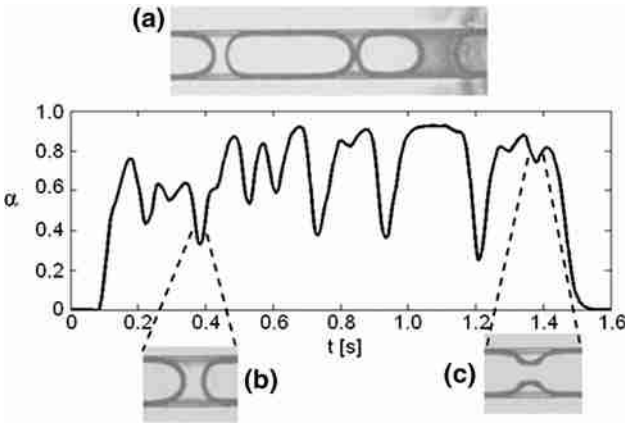

Fig. 10 The measured void fraction for a bubble train. (**a**) A typical bubble train. (**b**) Liquid slugs appear as sharp troughs in the signal. (**c**) Shallow troughs in the peaks are indicative of bubble coalescence

spaced bubbles and slugs might yield signals similar to a long slug with an unstable liquid film.

The void fraction signals generated by injecting air through the orifice at the center of the microchannel are rich with qualitative information about the evolution of the flows. Figure 10 is the Rhodamine 110 signal for a bubble train like the one depicted in image (a). The peaks represent individual bubbles or slugs. The sharp depressions are caused by the liquid slugs separating the bubbles. Image (b) is similar to the volume seen by the photodiodes. Larger liquid slugs yield deeper troughs. As the measurement volume decreases the measured void is more likely to reach zero as these liquid slugs pass by the sensors. A pair of closely spaced bubbles moving into the measurement volume will occasionally coalesce. When the bubbles merge the interface appears as the necking structure seen in image (c) and then expands to form the smooth interface characteristic of most long vapor bubbles. The small depressions in the peaks are characteristic of coalescing bubbles.

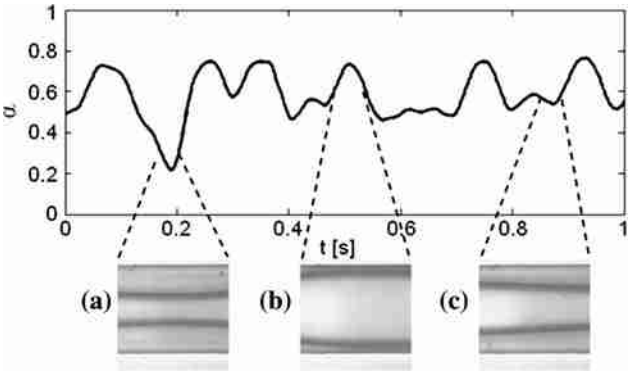

Fig. 11 The measured void fraction for a wavy annular flow. The void corresponds to the size of the vapor core which fluctuates from (**a**) narrow to (**b**) very large and (**c**) many values in between

Figure 11 shows a typical Rhodamine 110 signal for a wavy adiabatic gas–liquid annular flow. The peaks correspond to times when the vapor core fills most of the channel such as the flow in image (b). The measured void never reaches one as light emitted from the liquid in the corners and the thin liquid films surrounding the vapor core is captured. Images (a) and (c) portray the thinner vapor cores. The fluorescent technique is capable of capturing these fluctuations in the flow structure and provides an opportunity to quantitatively characterize the transient nature of the flows.

The wavy annular signal is rather similar to that of the bubble train in Fig. 10 and is susceptible to misinterpretation of the flow regime when pictures are not available. However, experienced individuals should be able to distinguish the differences. Bubble trains have sharper troughs than those seen in the annular flow signals. The annular flow rarely has time periods without void measured while bubble trains periodically indicate all liquid flow.

Since the fluorescent technique measures the void fraction associated with single bubbles, an array of fluorescent probes using optical fibers should yield even more information about two-phase flows in microchannels. Similar to the work of Ide et al. (2006), signal pairs can be cross-correlated to obtain slug length and velocity. Slug frequency can be readily obtained from the power spectrum. It may even be possible for slug growth rates to be extracted from a heavily arrayed channel.

Digital imaging in conjunction with fluorescence can yield even more information. As shown in Fig. 12, the intensity across cross section, A-A, which includes the wall, liquid, and vapor, is emitted from the liquid surrounding vapor bubbles. With proper calibration and illumination, the thickness of the liquid films around bubbles and slugs from images could be calculated.

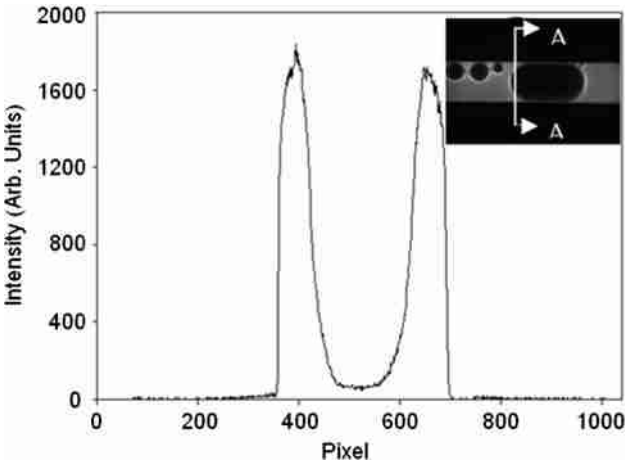

Fig. 12 Intensity measured across cross-section A-A

5.3 Temperature and liquid fraction measurements

The ability of this technique to simultaneously capture liquid temperature and void fraction is examined by adding air injection to the liquid temperature calibration process. The system is heated up to approximately 103°C. The power is turned off and the system is allowed to cool via natural convection. Throughout the cool down cycle, bubbles and slugs are injected through the air orifice in the center of the channel. The rapid fluctuations in the Rhodamine 110 signal over the duration of a run are shown in Fig. 9 along with the temperature as measured by the exit thermocouple.

The response of the fluorescent signal to changes in void fraction and temperature suggests the technique can eventually be utilized to accurately measure void fraction and temperature simultaneously. Unfortunately, as discussed below, the current uncertainty in the void fraction precludes such an approach. Future developmental efforts should focus on refining the void fraction measurement by mitigating sources of error including non-uniform illumination and wavelength dependent reflection and refraction.

Because temperature is calculated from the ratio of the signals, error in the temperature measurement increases at the lower liquid fractions. Assuming the independent measurements made by the photodiodes are slightly different, the ratio of the normalized powers becomes

$$\frac{\hat{P}_1}{\hat{P}_2} = \frac{\frac{\Phi_1(\mathsf{T})}{\Phi_1(\mathsf{T}_{\text{ref}})}(\beta+\varepsilon_1)}{\frac{\Phi_2(\mathsf{T})}{\Phi_2(\mathsf{T}_{\text{ref}})}(\beta+\varepsilon_2)} \tag{14}$$

where ε is the error in the liquid fraction for each signal. Rearranging this equation gives

$$\frac{\Phi_1(\mathsf{T})}{\Phi_2(\mathsf{T})} = \frac{\hat{P}_1}{\hat{P}_2}\frac{\Phi_1(\mathsf{T}_{\text{ref}})}{\Phi_2(\mathsf{T}_{\text{ref}})}\frac{(\beta+\varepsilon_2)}{(\beta+\varepsilon_1)} \tag{15}$$

This is the value used to obtain the temperature from the ratio of the calibration curves for the dye pair. The percent error in the term used to calculate temperature is given by

$$E = \left[\left(\frac{1+\varepsilon_2/\beta}{1+\varepsilon_1/\beta}\right) - 1\right] \times 100\% \tag{16}$$

Thus, as the liquid fraction β goes to zero, the magnitude of the error in the temperature measurement increases significantly when $\varepsilon_1 \neq \varepsilon_2$.

The resulting error in temperature for the current void fraction uncertainty of ±2% is too large to accommodate fully simultaneous measurement of temperature and void fraction. However, the current system does enable continuous quantification of void fraction with temperature measurements of the intermittent liquid slugs separating the vapor bubbles. Since Rhodamine 110 is relatively temperature insensitive, its fluorescent emission can be used to measure the void fraction. Knowing that the error in the temperature measurement becomes excessive as void fraction increases, temperature is only measured when the signal indicates the instantaneous void fraction is below 0.05.

Although average void fractions of 5% or less can hardly be considered two-phase flow, the instabilities and transient behavior characteristic of microchannel flow boiling offers many occasions where liquid nearly fills the measurement volume. Flow regimes comprised of individual bubbles, vapor slugs, and intermittent annular flows, all which have been observed in a number of two-phase microchannel studies (Thome 2004; Balasubramanian and Kandlikar 2005; Garimella et al. 2006; Kandlikar et al. 2006a, b), provide opportunities to measure the liquid temperature separating the individual vapor structures.

The data reduction process for the technique with intermittent temperature measurements is as follows:

1. Specify a voltage for each photodiode, $P(\mathsf{T}_{\text{ref}},\beta = 1)$, at a known temperature and liquid fraction of 1.
2. Evaluate the ratio, $\Phi_1(\mathsf{T})/\Phi_2(\mathsf{T})$, of the Rhodamine B signal to the Rhodamine 110 signal.
3. Obtain liquid temperature corresponding to the value of $\Phi_1(\mathsf{T})/\Phi_2(\mathsf{T})$ from the ratio of the calibration curves.
4. Using Eq. 7, evaluate the liquid fraction from the Rhodamine 110 signal where the values of T are the temperatures obtained in Step (3).
5. Reject all values of temperature for liquid fractions less than 0.95.
6. Linearly interpolate the temperature signal to obtain estimates of the liquid temperature for the points rejected in Step (5).
7. Obtain new values of the liquid fraction using Eq. 7 and the updated temperatures from Step (6).

Figure 13 compares the temperature measured by the fluorescent technique to the exit thermocouple temperature

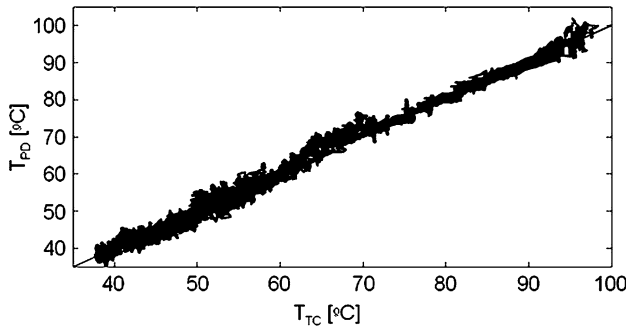

Fig. 13 Comparison of the temperature measured with the thermocouple versus the photodiodes for the calibration procedure with air injection

for the calibration process with air injection. The data reduction process described above yields good agreement with the thermocouple measurements. The two measurements are within ±3°C with 95% confidence.

6 Conclusions

The dependence of light emission by a fluorescent dye on temperature and void fraction has been leveraged to develop a non-invasive two-dye/two-color technique capable of measuring liquid temperature and void fraction in certain microchannel two-phase flows. Theory indicates fully simultaneous measurements of both parameters are possible, however, in practice uncertainty in the measured void fraction can lead to significant error in the temperature measurement as the void fraction approaches unity. Given the uncertainty for void fraction (2%) in the current setup, an alternative to the ideal data reduction scheme has been proposed which yields liquid temperatures for times when the measurement volume is nearly all liquid. Using Rhodamine 110 and Rhodamine B, the temperature of intermittent liquid slugs measured using fluorescence in a bubbly/slug flow agreed to with ±3°C of thermocouple data over a temperature range from 35 to 100°C. The relative insensitivity of Rhodamine 110 to temperature allows continuous quantification of the void fraction.

This technique provides an opportunity to significantly expand the set of flow parameters that can easily be measured in microchannels. Using quantitative point sensor data rather than digital images can help refine flow regime classification by relating transitions to bubble/slug frequency or measured void fraction. The development of arrays of fluorescent probes will allow parameters such as slug size, velocity, and growth to be measured through the cross-correlation of neighboring signals. Fluorescence coupled with CCD imaging can yield values for the thickness of the liquid films surrounding bubbles. Arrays of probes will be also very useful in understanding the complex flow patterns associated with parallel channel instabilities. Additional work is required before the full potential of this metrology is realized.

Acknowledgments The research was performed under appointment to the Naval Nuclear Propulsion Fellowship Program sponsored by Naval Reactors Division of the US Department of Energy. We also acknowledge support from the MARCO Interconnect Focus Center, and from the Stanford Graduate Fellowship Program.

References

Angelini S, Quam W et al (1992) FLUTE-fluorescent technique for two-phase-flow liquid fraction measurements. Chem Eng Comm 118:237–249

Balasubramanian P, Kandlikar SG (2005) Experimental study of flow patterns pressure drop, and flow instabilities in parallel rectangular minichannels. Heat Trans Eng 26(3):20–27

Barton DI, Tangyunyong P (1996) Fluorescent microthermal imaging—theory and methodology for achieving high thermal resolution images. Microelectron Eng 31:271–279

Bazile R, Stepowski D (1994) Measurements of the vaporization dynamics in the development zone of a burning spray by planar laser induced fluorescence and Raman scattering. Exp Fluids 16:171–180

Bruchhausen M, Guillard F, Lemoine F (2005) Instantaneous measurement of two-dimensional temperature distributions by means of two-color planar laser induced fluorescence (PLIF). Exp Fluids 38:123–131

Brunschwiler T, Rothuizen H et al (2006) Direct liquid jet-impingement cooling with micron-sized nozzle array and distributed retrun architecture. In: 20th ITHERM conference, San Diego, California

Chaouki J, Larachi F, Dudukovic MP (1997) Non-invasive monitoring of multiphase flows. Elsevier, New York

Fogg D, Flynn R et al (2004) Fluorescent imaging of void fraction in two-phase microchannels. In: 3rd interntional symposium on two-phase flow modeling and experimentation, Pisa, Italy

Garimella SV, Singhal V, Liu D (2006) On-chip thermal management with microchannel heat sinks and integrated micropumps. Proc IEEE 94(8):1534–1548

Guilbault GG (1990) Practical fluorescence. Marcel Dekker, New York

Hollingsworth DK (2004) Liquid crystal imaging of flow boiling in minichannels microchannels. Rochester, New York

Ide H, Kimura R, Kawaji M (2006) Optical measurement of void fraction and bubble size distribution in a microchannel. In: 4th international conference on nanochannels microchannels minichannels, Limerick, Ireland

Jacobi AM, Thome JR (2002) Heat transfer model for evaporation of elongated bubble flows in microchannels. J Heat Trans 124:1131–1136

Kandlikar SG, Garimella S et al (2006a) Heat transfer and fluid flow in minichannels and microchannels. Elsevier, London

Kandlikar SG, Kuan WK et al (2006b) Stabilization of flow boiling in microchannels using pressure drop elements and fabricated nucleation sites. J Heat Trans 128:389–396

Keska JK (2005) An application of concomitant measurements for two-phase flow of air–water mixture in minichannels. In: 3rd international conference microchannels minichannels, Toronto, Canada

Kim HJ, Kihm KD, Allen JS (2003) Examination of ratiometric laser induced fluorescence thermometry for microscale spatial measurement resolution. Int J Heat Mass Trans 46(21):3967–3974

Koo J-M, Jiang L et al (2001) Modeling of two-phase microchannel heat sinks for VLSI chips. Microelectromechanical Systems, Interlaken, Switzerland

Kosar A, Kuo C-J, Peles Y, Jensen MK (2005) Enhanced boiling heat transfer in second generation microchannels part a: methods and preliminary results. In: 3rd international conference microchannels minichannels, Toronto, Canada

Lavieille P, Delconte A et al (2004) Non-intrusive temperature measurements using three-color laser-induced fluorescence. Exp Fluids 36:706–716

Lavieille P, Lemoine F et al (2001) Evaporating and combusting droplet temperature measurements using two-color laser-induced fluorescence. Exp Fluids 31:45–55

Lee M, Wong M, Zohar Y (2003) Characterization of an integrated micro heat pipe. J Micromech Microeng 13:58–64

Mallik AK, Peterson GP, Weichold MH (1992) On the use of micro heat pipes as an integral part of semiconductor devices. ASME J Electron Packag 114:436–442

Maqua C, Castanet G et al (2006) Temperature measurements of binary droplets using three-color laser-induced fluorescence. Exp Fluids 40:786–797

Narayanan V (2003) Temperature measurements and surface visualization in microchannel flows using infrared thermography. In: 1st international conference on microchannels minichannels, Rochester, New York

Qu W, Mudawar I (2003) Flow boiling heat transfer in two-phase micro-channel heat sinks-II. Annular two-phase flow model. Int J Heat Mass Trans 46:2773–2784

Ross D, Gaitan M, Locoscio LE (2001) Temperature measurement in microfluidic systems using a temperature-dependent fluorescent dye. Anal Chem 73:4117–4123

Sakakibara J, Adrian RJ (1999) Whole field measurement of temperature in water using two-color laser induced fluorescence. Exp Fluids 26:7–15

Sakakibara J, Adrian RJ (2004) Measurement of temperature field of a Rayleigh–Benard convection using two-color laser-induced fluorescence. Exp Fluids 37:331–340

Thome JR (2004) Boiling in microchannels: a review of experiment and theory. Int J Multiph Flow 25:128–139

Tong LS (1995) Boiling heat transfer and two-phase flow. Krieger Pub, New York

Wang EN, Zhang L et al (2002) Micromachined jet arrays for liquid impingement cooling of VLSI chips. Hilton Head 2002: solid-state sensors and actuators workshop. Hilton Head, SC, USA

Wu HY, Cheng P (2003) Visualization and measurements of periodic boiling in silicon microchannels. Int J Heat Mass Trans 46:2603–2614

Wu HY, Cheng P (2004) Boiling instability in parallel silicon microchannels at different heat flux. Int J Heat Mass Trans 47:3631–3641

Xu JL, Zhou JJ et al (2004) Unsteady flow phenomenon in a heated microchannel at high heat fluxes. Exp Heat Trans 17:299–319

Yarin LP, Ekelchik LA, Hetsroni G (2002) Two-phase laminar flow in a heated microchannels. Int J Heat Mass Trans 28:1589–1616

Zhang L, Koo J-M et al (2002) Measurements and modeling of two-phase flow in microchannels with nearly-constant heat flux boundary conditions. J Microelectromech Sys 11:12–19